

1 **Constraints on absolute chamber volume from geodetic**  
2 **measurements: Trapdoor faulting in the Galapagos**

3 **Yujie Zheng<sup>1</sup>, Laura Blackstone<sup>2</sup>, Paul Segall<sup>2</sup>**

4 <sup>1</sup>Division of Geological and Planetary Sciences, California Institute of Technology

5 <sup>2</sup>Geophysics Department, Stanford University

6 **Key Points:**

- 7 • The best fitting trapdoor faults are near vertical and dip steeply to the north (88  
8 degree).
- 9 • An upper bound on chamber volume is between 13.6 km<sup>3</sup> and 20.6 km<sup>3</sup>, depend-  
10 ing on fault dip.
- 11 • The lower bound on volume is one-half the upper bound.

---

Corresponding author: =name=, =email address=

## Abstract

Magma chamber volume is critical for volcano monitoring and forecasting. Standard geodetic methods cannot constrain the total volume, only the change in volume. Here, we show that stress perturbations associated with trapdoor faulting allow for bounds to be placed on the total chamber volume at Sierra Negra volcano, in the Galapagos. The deformation response of the magma chamber to faulting depends on both the absolute chamber volume and the compressibility of the magma. Bubble-free magma provides the lower limit on compressibility, thus an upper bound on the chamber volume of 13.6 to 20.6 km<sup>3</sup>, depending on fault dip. We estimate an upper limit on compressibility using a conduit model relating volatile content to lava fountain height, which is compared with observations from the 2005 eruption, constrained by volatile content of olivine melt inclusions. This yields a lower bound on chamber volume of  $0.5 \times$  the upper bound.

## Plain Language Summary

It is important to understand the size of subterranean magma reservoirs since the volume of available magma bounds the size of short-lived eruptions. In this study, we analyze unique trapdoor faulting earthquakes observed at the Sierra Negra volcano. These events last only a few seconds and cause unique displacements of the ground surface. The volume change and magma pressure drop due to trapdoor faulting depend on the product of chamber volume and magma compressibility. The lower limit of the compressibility is for bubble-free magma. We estimate an upper bound by using observations of “fire fountain” heights during the 2005 eruption. Higher gas content, and thus more compressible magma, lead to higher fire fountains. We find an upper bound on the magma volume of 13.6 km<sup>3</sup> to 20.6 km<sup>3</sup>, depending on fault dip. We also find that the observed fire fountain height can be fit with plausible H<sub>2</sub>O content and up to 0.15 weight % CO<sub>2</sub>, which leads to a lower bound of magma volume of one-half the upper bound. Our results will be an important benchmark for comparison with other methods of estimating magma chamber volume and form a useful constraint for other similar volcanoes worldwide.

## 1 Introduction

The volume of magma reservoirs is critical for volcano monitoring and forecasting. The total volume provides an upper bound on the possible eruptive volume, assuming

43 no recharge during the eruption. Knowledge of subsurface magma volumes also helps con-  
44 strain models of magma chamber evolution. However, determining the total chamber vol-  
45 ume from geophysical methods has been challenging. Seismic tomography can map the  
46 distribution of wave speeds and attenuation, but employing these results to estimate vol-  
47 umes of melt is not straightforward (Lees, 2007; Paulatto et al., 2012; Rawlinson et al.,  
48 2014). The same is true for electromagnetic imaging. The distribution of earthquake hypocen-  
49 ters can provide a qualitative sense of magma chamber volume, but location uncertainty  
50 and the potential for hot, aseismic rock surrounding magma reservoirs limit quantita-  
51 tive analysis. Geochemical mixing models can provide estimates of the volume of the well-  
52 mixed portion of shallow reservoirs (D. Geist et al., 2002; Pietruszka & Garcia, 1999).

53 Standard geodetic models constrain the *change* in chamber volume but place weak  
54 if any constraints on total chamber volume (Segall, 2013). This is well expressed, for ex-  
55 ample, in the “Mogi model” (Yamakawa, 1955; Mogi, 1958), in which the amplitude of  
56 surface deformation is proportional to the product of the pressure change  $\Delta p$  and the  
57 total volume  $V$ , and inversely proportional to the shear modulus  $\Delta p V / \mu$ .

58 The absolute chamber volume can be inferred from geodetic observations if there  
59 are independent constraints on pressure change. Such analyses have been conducted at  
60 Kīlauea volcano, where active lava lakes were hydraulically connected to the summit cham-  
61 ber, such that changes in lava level can be interpreted as changes in chamber pressure  
62 (Johnson, 1992; Denlinger, 1997; Segall et al., 2001; Anderson et al., 2015). Estimates  
63 using this approach range from 240 km<sup>3</sup> for the entire magmatic system, including the  
64 rift zones (Denlinger, 1997), to 20 km<sup>3</sup> for the summit chamber (Segall et al., 2001), to  
65 as low as  $\sim 1$  km<sup>3</sup> for the shallow Halema’uma’u source of episodic deflation-inflation  
66 events (Anderson et al., 2015). Most recently, Anderson et al. (2019) combined the re-  
67 markable drainage of the summit lava lake during the early stage of the 2018 eruption  
68 with Global Positioning System (GPS), tilt, and Interferometric Synthetic Aperture Radar  
69 (InSAR) data to constrain the volume of the summit Halema’uma’u reservoir to between  
70 2.5 to 7.2 km<sup>3</sup> at 68% confidence bounds. This work shows that it is possible to deter-  
71 mine the total magma chamber volume even without open conduits from the chamber  
72 to the surface. In particular, we show that perturbations in stress associated with trap-  
73 door faulting events allow bounds to be placed on the total volume of the magma cham-  
74 ber at Sierra Negra volcano in the Galapagos.

75 Sierra Negra is the largest and the most voluminous of the six actively deforming  
76 volcanoes in the western Galapagos islands, with the most recent eruption in 2018 (Vasconez  
77 et al., 2018; Bell et al., 2021). Inflation at Sierra Negra has been punctuated by several  
78 trapdoor faulting events, with slip occurring along a complex set of intra-caldera faults  
79 with outward dipping fault scarps (Figure 1) along the southern and western margin of  
80 the caldera (Reynolds et al., 1995). The first indication of trapdoor faulting came from  
81 InSAR observations spanning 1997-98 and is thought to be associated with a  $M_w$  5.0 event  
82 on 11 January 1998 (Amelung et al., 2000; Jónsson et al., 2005). A second trapdoor fault-  
83 ing event, associated with a  $m_b$  4.6 earthquake was well captured by both InSAR and  
84 GPS data on 16 April 2005 (Chadwick et al., 2006; Jónsson, 2009). The GPS station GV06  
85 was uplifted by almost one meter within 10 seconds during this event. In comparison,  
86 the prior inflation rate at Sierra Negra was approximately 0.1 cm/day (Chadwick et al.,  
87 2006). The short duration implies that negligible amounts of magma left or entered the  
88 chamber during the faulting event. Both the 2005 and the 2018 eruptions were also pre-  
89 ceded by trapdoor faulting events (Chadwick et al., 2006; S.-H. Yun, 2007; Vasconez et  
90 al., 2018), suggesting they influenced the subsequent eruptions.

91 Here we analyze both GPS and InSAR data for the trapdoor faulting event on 16  
92 April 2005. The mechanical response of the magma chamber to the trapdoor faulting  
93 depends on the product of the total chamber volume and magma compressibility and  
94 is clearly expressed in the surface deformation. We show that by constraining the rel-  
95 ative compressibility of the magma and the magma chamber it is possible to constrain  
96 the absolute volume of the shallow magma reservoir.

## 97 **2 Method**

98 This section presents a 3D fault-chamber model in an elastic half space to demon-  
99 strate the interaction between trapdoor faulting and the magma chamber. Before a trap-  
100 door event, magma influx leads to increased pressure and inflationary deformation with-  
101 out fault slip. During the trapdoor event the fault slips while the mass of magma within  
102 the chamber remains unchanged. Magma migrates within the reservoir on the time scale  
103 of the faulting event to eliminate pressure gradients generated by the sudden fault slip.

104 Models of Sierra Negra based on GPS and InSAR data have indicated a sill-like  
105 chamber with its top at a depth of about 2 km, though a diapir with a flat top also pro-  
106 vides an adequate fit (S. Yun et al., 2006; Amelung et al., 2000; Chadwick et al., 2006).

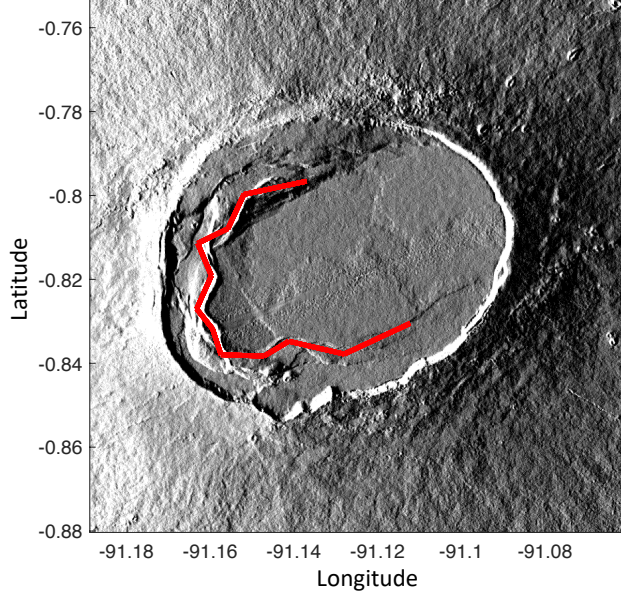


**Figure 1.** Shaded relief map of the Sierra Negra Volcano showing the intra-caldera fault system (thick red lines).

107 We assume that the sill surfaces are uniformly pressurized with no shear traction, con-  
 108 sistent with the assumption of nearly static fluid. We use the Displacement Discontinuity  
 109 Method (DDM) to model a crack-like sill. The boundary conditions on the sill are  
 110 specified by

$$\underline{\sigma} = H\underline{\delta} + H_1\underline{s} = -\Delta p\underline{1} \quad (1a)$$

$$\underline{\tau}_x = J_{1x}\underline{s} + J_{2x}\underline{\delta}_x + J_{3x}\underline{\delta}_y = \underline{0} \quad (1b)$$

$$\underline{\tau}_y = J_{1y}\underline{s} + J_{2y}\underline{\delta}_x + J_{3y}\underline{\delta}_y = \underline{0} \quad (1c)$$

111 where  $\underline{\sigma}$ ,  $\underline{\tau}_x$  and  $\underline{\tau}_y$  are the normal and horizontal shear tractions in the  $x$  and  $y$  direc-  
 112 tions on the sill surface, respectively.  $\underline{\delta}$  is the opening of the sill,  $\underline{s}$  is a vector of fault slips,  
 113 and  $\underline{\delta}_x$  and  $\underline{\delta}_y$  represent shear displacement discontinuities (dislocations) of the sill in  
 114 the  $x$  and  $y$  directions.  $\Delta p$  represents perturbation of pressure on the walls of the magma  
 115 chamber associated with trapdoor faulting, and  $\underline{1}$  is a vector of ones. Matrices  $H$  and  
 116  $H_1$  map displacements into normal stress and matrices  $J_{ix}$ ,  $J_{iy}$ ,  $i = 1, 2, 3$  map displace-  
 117 ments into shear stress; all are computed using results for rectangular and triangular dis-  
 118 locations in a homogeneous elastic half-space (Okada, 1992; Maerten et al., 2005).

119 Kinematic conditions link the slip at the bottom of the fault to openings at the edge  
 120 of the sill adjacent to the fault,

$$N_z B \underline{s} = E \underline{\delta} \quad (2a)$$

$$N_x B \underline{s} = E \underline{\delta}_x \quad (2b)$$

$$N_y B \underline{s} = E \underline{\delta}_y \quad (2c)$$

121 where  $B$  and  $E$  are matrices that extract elements associated with the bottom of the fault  
 122 and the edge of the sill, respectively.  $N_z$ ,  $N_x$  and  $N_y$  are matrices that extract vertical,  
 123 east-west, and north-south components of displacements at the bottom of the fault.

The volume change of the magma chamber during a faulting event is found by in-  
 tegrating the opening,  $\underline{\delta}$ , over the surface of the sill, which can be written compactly as

$$\Delta V = \Psi \Delta p + \Phi \cdot \underline{s} \quad (3)$$

124 where  $\Psi = (dV/dp)_s$  is the volume change per unit pressure change with no slip on the  
 125 fault and  $\Phi \cdot \underline{s}$  is the volume change for unit slip at constant pressure.  $\Psi$  is related to  
 126 the chamber compressibility,  $\beta_c = (1/V) (dV/dp) = \Psi/V$ . Derivations of  $\Psi$  and  $\Phi$  are  
 127 given in Supplementary Materials. The first term of Eqn. [3] represents chamber vol-  
 128 ume change related to stress perturbation caused by trapdoor faulting. The second term  
 129 gives the direct volume change caused by forced opening at the edge of the sill due to  
 130 trapdoor faulting.

Since the trapdoor faulting event took place over a few seconds, negligible magma  
 could have entered or exited the chamber. A linearized description of the mass change  
 gives

$$\Delta m / \rho = V \beta_m \Delta p + \Delta V = 0 \quad (4)$$

131 where  $\rho$  and  $\beta_m$  are the magma density and compressibility, respectively.

132 Equations of mass conservation [4] and elasticity [3] provide two independent re-  
 133 lations between volume and pressure changes during the faulting event. Combining them  
 134 yields

$$\Delta p = \frac{-\Phi \cdot \underline{s}}{V \beta_m + \Psi}, \quad (5a)$$

$$\Delta V = \frac{V \beta_m (\Phi \cdot \underline{s})}{V \beta_m + \Psi}. \quad (5b)$$

Note that in the limit of small chamber volume and/or incompressible magma,  $V \beta_m \rightarrow$   
 0, that  $\Delta V \rightarrow 0$ , while  $\Delta p \rightarrow -\Phi \cdot \underline{s} / \Psi$ . On the other hand in the limit of large vol-

ume and/or very compressible magma,  $V\beta_m \rightarrow \infty$ , that  $\Delta p \rightarrow 0$  and  $\Delta V \rightarrow \Phi \underline{s}$ . This shows that the volume change of the magma chamber, which can be detected geodetically, is sensitive to the absolute chamber volume and the magma compressibility. Rewriting equation [5a],

$$V = -\frac{1}{\beta_m} \left( \Psi + \frac{\Phi \cdot \underline{s}}{\Delta p} \right). \quad (6)$$

135 Note that  $\Delta p \leq 0$  (from 5a) and the term in parentheses in [6] is negative, such that  
136  $V > 0$ .

The surface displacements  $\underline{u}$  resulting from the fault-chamber interaction can also be expressed in terms of a vector of slips along the trapdoor fault  $\underline{s}$ , and a scalar pressure change in the magma chamber  $\Delta p$ ,

$$\underline{u} = G_p \Delta p + G_s \underline{s}, \quad (7)$$

137 where  $G_p$  and  $G_s$  are computed from rectangular and triangular elastic dislocations. Es-  
138 timates of  $\Delta p$  and  $\underline{s}$  from geodetic measurements, obtained by inverting equation [7], can  
139 be used in equation [6] together with  $\Psi$  and  $\Phi$ , which are determined by elasticity cal-  
140 culations given the fault and chamber geometry (Eqn.[4] and [5] in Supplementary Ma-  
141 terial). Thus, with bounds on  $\beta_m$  we can bound the absolute magma chamber volume  
142  $V$ .

### 143 **3 Results**

We use GPS and InSAR data (from Jónsson (2009)) to estimate the fault slip (as-  
suming pure dip-slip) and pressure change in the magma chamber using Eqn. [7]. The  
InSAR data has been corrected for inflation during the time span of the SAR acqui-  
sitions, both before and after the trap-door faulting. To avoid over-fitting, we smooth the  
solution by minimizing the second derivative of the fault slip. Specifically we minimize  
the objective function:

$$F(\Delta p, \underline{s}) = (\underline{u}_{insar} - \hat{\underline{u}}_{insar})^T \Sigma_{insar}^{-1} (\underline{u}_{insar} - \hat{\underline{u}}_{insar}) + w^2 (\underline{u}_{gps} - \hat{\underline{u}}_{gps})^T \Sigma_{gps}^{-1} (\underline{u}_{gps} - \hat{\underline{u}}_{gps}) + \alpha^2 \|L \hat{\underline{s}}\|_2^2, \quad (8)$$

144 where  $\hat{\underline{u}}$  is the predicted data,  $L$  is the second derivative operator,  $\Sigma_{insar}$  and  $\Sigma_{gps}$  are  
145 covariance matrices of InSAR and GPS data, respectively. We use data from the non-

146 deforming areas north of the caldera to construct an empirical isotropic covariance ma-  
 147 trix  $\Sigma_{insar}$  (Fig.S1). Correlation between GPS measurements are assumed to only ex-  
 148 ist between horizontal components. The choice of the smoothness parameter  $\alpha^2$  is based  
 149 on an “L-curve” (Fig. S2). We weight the GPS data by  $w^2$  to account for the dispar-  
 150 ity between the number of GPS data points and the number of InSAR data points. We  
 151 chose a weight factor of  $w = 5$  so that fits to both GPS and InSAR data are satisfac-  
 152 tory (Fig. S3). We assume a shear modulus of  $\mu = 10$  GPa and Poisson’s ratio  $\nu =$   
 153 0.25.

154 Previous inversions have well constrained the location and the shape of the cham-  
 155 ber during inflationary episodes. We fix the sill geometry as described in S. Yun et al.  
 156 (2006). To determine the fault dip, we tested a range of dips from outward dipping  $70^\circ$   
 157 to inward dipping  $70^\circ$ , constraining the bottom edge of the fault to be aligned with the  
 158 edge of the sill. The misfit as a function of dip (Fig. 2a) is discontinuous because vary-  
 159 ing the dip changes the projection of the surface expression of the fault. We find that  
 160 inward (northward) dips of  $80$  to  $90^\circ$  provide reasonable fits to both InSAR and GPS  
 161 data, with a near-vertical,  $88^\circ$  dip being optimal. In contrast, Chadwick et al. (2006) and  
 162 Jónsson (2009) concluded the best-fitting faults are more shallowly inward dipping ( $71^\circ$ ),  
 163 although their calculations use a single planar fault and do not account for the presence  
 164 of the magma chamber. We thus set the fault north dipping at  $88^\circ$  and only allow dip-  
 165 slip on the fault. Fig. 2b shows the estimated fault slip and the amount of sill opening  
 166 or closing. Note that the northern edge of the sill, opposite from the sector of the fault  
 167 with maximum slip, is predicted to have closed. The estimated pressure change in the  
 168 chamber is  $-0.8$  MPa.

169 Fig. 3 shows the observed and predicted InSAR and GPS displacements. The pre-  
 170 ferred model can match both GPS and InSAR data quite well. In particular, the model  
 171 accounts for the modest subsidence observed at the north edge of the caldera – oppo-  
 172 site from the fault segment that experienced the most slip. Previous studies could not  
 173 capture the observed subsidence with a model restricted to fault slip and not including  
 174 the magma reservoir (Chadwick et al., 2006; Jónsson, 2009). In addition, our model can  
 175 explain most of the horizontal displacements recorded in the GPS data without requir-  
 176 ing strike-slip motion on the trapdoor fault.

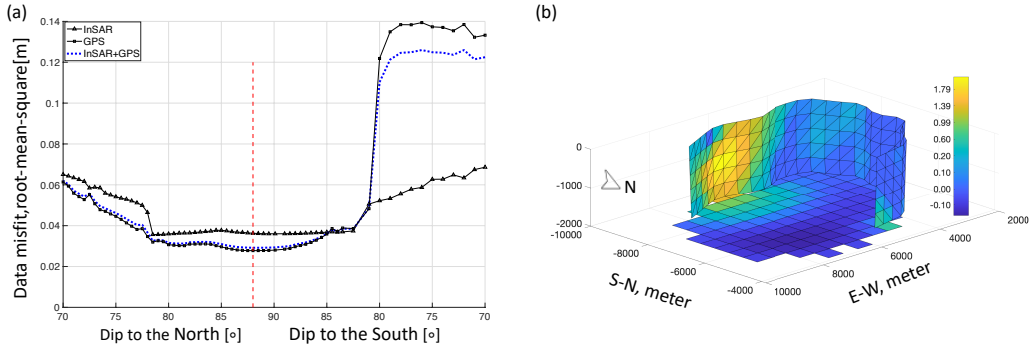


**Figure 2.** (a) Misfits of GPS (circles), InSAR (triangles) and their weighted combination (blue dotted line) as a function of fault dip. The vertical red line shows the optimal fault dip. (b) Estimated fault slip distribution and sill openings in meters with a fault dip of  $88^\circ$  to the North. Only dip slip is allowed on the fault.

## 177 4 Discussion

### 178 4.1 Upper Bound on Volume

179 The product  $V\beta_m$  is estimated to be  $1.7 \text{ m}^3/\text{Pa}$ . In comparison, Anderson et al.  
 180 (2019) estimate this product to be  $1.3 - 5.5 \text{ m}^3/\text{Pa}$  (95% bounds) from deformation and  
 181 lava lake drainage during the early phase of the 2018 Kilauea eruption. Segall and An-  
 182 derson (2021) model episodic caldera collapse during the caldera forming phase of the  
 183 2018 eruption and find a range of  $1.4 - 4.1 \text{ m}^3/\text{Pa}$ . The estimate for Sierra Negra falls  
 184 at the lower end of the range for Kilauea.

185 Sierra Negra lavas are tholeiitic basalts. For bubble-free free basalt, which repre-  
 186 sents a lower bound on the compressibility, experimental results of Murase and McBir-  
 187 ney (1973) yield  $\beta_m \approx 10^{-10} \text{ Pa}^{-1}$ . The thermodynamic model MELTS (Gualda et al.,  
 188 2012; Ghiorso & Gualda, 2015) yields  $\beta_m \approx 5.6 \times 10^{-11} \text{ Pa}^{-1}$  for bubble-free basalt of  
 189 Sierra Negra composition, roughly a factor of two less than the experimental value. Un-  
 190 less noted, we refer to the experimental value but acknowledge a factor of two uncertainty  
 191 in this parameter. With the bubble-free experimental value of magma compressibility  
 192  $\beta_m$ , we obtain an upper bound on the absolute chamber volume of  $V \sim 17.4 \text{ km}^3$ , cor-  
 193 responding to a maximum sill thickness of  $\sim 623 \text{ m}$ , given the areal extent of the sill.

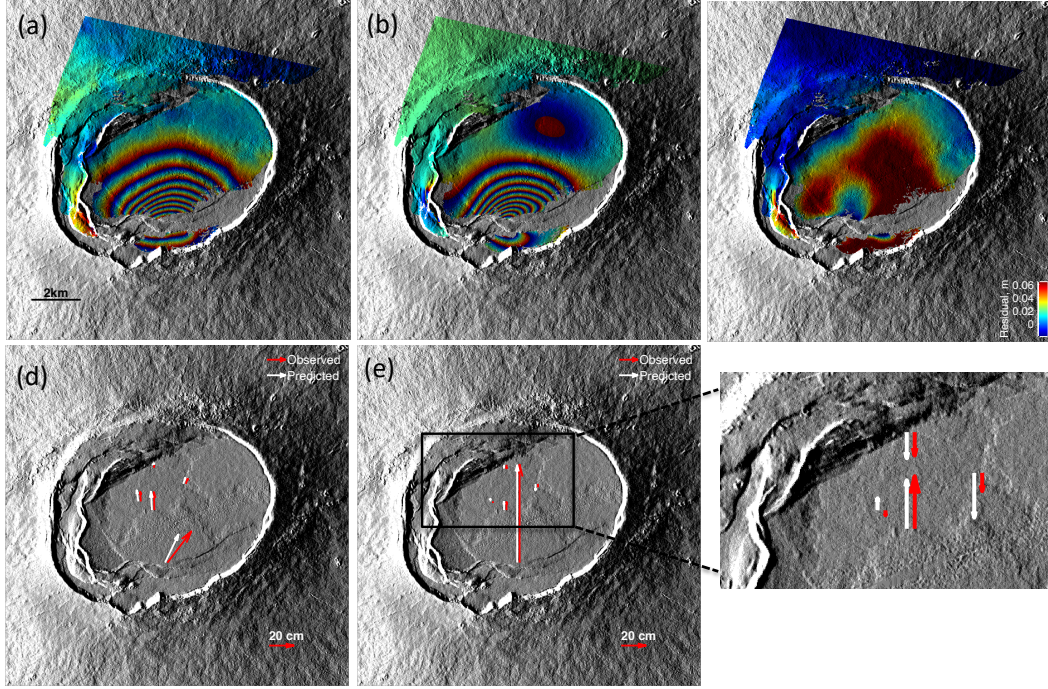


**Figure 3.** (a) Observed and (b) predicted InSAR data from the trapdoor-chamber model shown in Fig. 2(b), re-wrapped at 10 cm fringes. (c) Residuals between observed and predicted InSAR data. (d) Observed and predicted GPS horizontal displacements. (e) Observed and predicted GPS vertical displacements. The inset shows subsidence of the northernmost stations.

194           Given the high InSAR and GPS measurements quality, uncertainties in chamber  
 195 volume  $V$  (Eq.[6]) mainly stem from uncertainties in the adopted fault-chamber geom-  
 196 etry, the choice of elastic constants, and estimates of magma compressibility. We address  
 197 each of these factors in the following.

198           Inversions of data from previous inflationary episodes have shown that Sierra Ne-  
 199 gra has a sill-like chamber (S. Yun et al., 2006; Amelung et al., 2000). However, geode-  
 200 tic data is not sensitive to the shape of the chamber as long as the chamber has a flat  
 201 top. Estimation of the chamber volume  $V$  depends on the parameter  $\Psi$ , which describes  
 202 the compressibility of the chamber and is determined by elasticity calculations given the  
 203 chamber geometry. Perhaps unintuitively, the thickness of the sill has a limited impact  
 204 on  $\Psi$ ; The same is not true for  $\beta_c$ . For a penny-shaped sill at 2 km depth with radius  
 205  $a = 3$  km in an elastic half-space with  $\mu = 10$  GPa, we compute  $\Psi = 9.1$  m<sup>3</sup>/Pa. In  
 206 contrast, for a spherical chamber with radius small compared to its depth (the Mogi model)

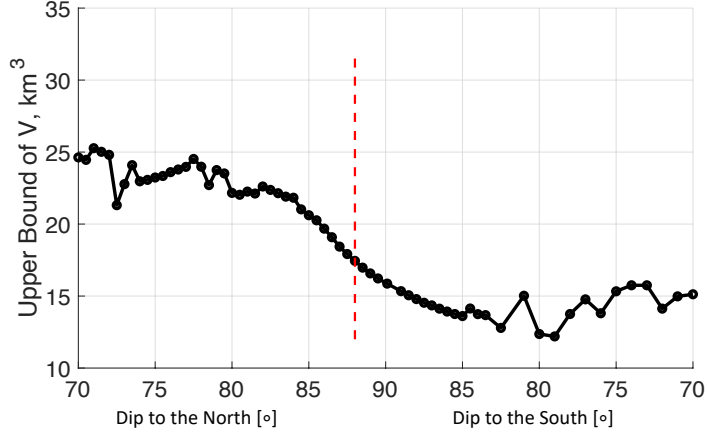


**Figure 4.** Estimated upper bound of chamber volume as a function of fault dip, assuming a magma compressibility of  $10^{-10} \text{ Pa}^{-1}$ . The red dashed vertical line indicates the optimal fault dip.

207  $\Psi \equiv dV/dP = \pi a^3/\mu$ . With the same values of  $a$  and  $\mu$ ,  $\Psi = 8.48 \text{ m}^3/\text{Pa}$ , a differ-  
 208 ence of only 6%.

209 Estimation of  $\Phi \cdot s/\Delta p$ , and therefore the estimated reservoir volume, depends on  
 210 fault dip. Fig. 4 illustrates how the estimated upper bound on volume varies with fault  
 211 dip. Varying the fault dip from  $85^\circ \text{ S}$  to  $85^\circ \text{ N}$ , the estimated upper bound of chamber  
 212 volume ranges from  $13.6 \text{ km}^3$  to  $20.6 \text{ km}^3$ . Over this same range of dips, the estimated  
 213 pressure change within the magma chamber due to trapdoor faulting ranges from  $-0.81$   
 214 MPa to  $-0.93 \text{ MPa}$ . The relatively small pressure drop on the chamber is consistent with  
 215 the observation that the trapdoor faulting event did not significantly perturb the infla-  
 216 tion rate (Chadwick et al. (2006), Fig.1D). If the pressure drop had been larger, we might  
 217 have expected an increase in the inflation rate relative to the pre-faulting rate. The trap-  
 218 door faulting event before the 2018 eruption similarly does not significantly impact the  
 219 uplift rate (Bell et al., 2021).

## 220 4.2 Lower Bound on Volume

221 An upper bound on magma compressibility, and hence a lower bound on chamber  
 222 volume, is obtained by determining the maximum plausible exsolved  $\text{CO}_2$  and  $\text{H}_2\text{O}$  vol-  
 223 ume fraction within the chamber. Following previous studies (Gerlach & Graeber, 1985;

224 Parfitt et al., 1995; Wasser et al., 2021), we use two sets of observations: melt inclusions  
 225 and observed eruption fountain heights.

226 Koleszar et al. (2009) analyze olivine melt inclusions from Fernandina lavas sim-  
 227 ilar to those at Sierra Negra. The most volatile-enriched melt inclusions, which are as-  
 228 sumed to be representative of primitive mantle-derived magmas, contain up to 6000 ppm  
 229 CO<sub>2</sub> and 1.1 wt. % H<sub>2</sub>O. More typical samples, assumed to be representative of magma  
 230 during crustal storage, contain 200 to 600 ppm CO<sub>2</sub> and 0.5 to 1.1 wt. % H<sub>2</sub>O. Peterson  
 231 et al. (2017) provide compositions for submarine glasses similar in composition and prox-  
 232 imity to Sierra Negra with volatile contents ranging from 20 to 188 ppm CO<sub>2</sub> and 0.49  
 233 to 1.15 wt. percent H<sub>2</sub>O. These glasses come from lavas that erupted on the sea floor  
 234 and are thought to be continuously re-equilibrated during ascent.

235 We use the equilibrate function of MELTS (Gualda et al., 2012; Ghiorso & Gualda,  
 236 2015) on a typical Sierra Negra composition from Peterson et al. (2017) with the max-  
 237 imum observed CO<sub>2</sub> content of 6000 ppm from Koleszar et al. (2009), at pressure and  
 238 temperature conditions for a chamber 2 km deep. The resulting magma compressibil-  
 239 ity is  $\sim 1.5 \times 10^{-9} \text{ Pa}^{-1}$  (Figure 5B), a 15 fold increase in  $\beta_m$  relative to bubble-free  
 240 melt. This is an extreme bound on compressibility since some loss of CO<sub>2</sub> from the cham-  
 241 ber is certain between eruptions. Taking  $\sim 600$  ppm CO<sub>2</sub> as a more plausible upper bound  
 242 on CO<sub>2</sub> content within the chamber results in a compressibility of  $\sim 1.3 \times 10^{-10} \text{ Pa}^{-1}$ ,  
 243 a 1.3 fold increase in  $\beta_m$  relative to the bubble-free melt.

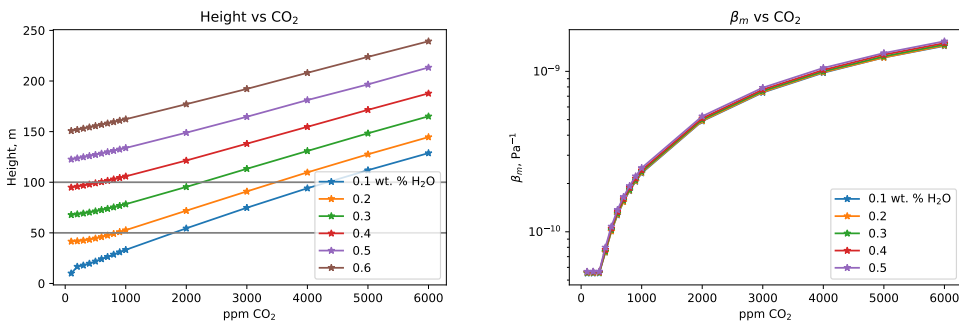


**Figure 5.** Dependence of fountain height on volatile content. A) Fountain height as a function of CO<sub>2</sub> content, for various water contents. Horizontal lines mark fountain height of 50 and 100 m. The volume flux is constrained to 100 m<sup>3</sup>/s. B) Magma compressibility  $\beta_m$  as a function of CO<sub>2</sub> content, for various water contents.

244 The second approach uses an eruption conduit model to relate volatile content to  
245 observed lava-fountain height during the 2005 Sierra Negra eruption that followed a trap-  
246 door faulting event. D. J. Geist et al. (2008a) report fountain heights of up to 300 m on  
247 the second day of the eruption. Days 3-6 saw two primary fountains with heights of 30  
248 m and 50 m. On day 7 a single fountain was observed with a height of 50 m. The es-  
249 timated volume flux at this time was  $\sim 100 \text{ m}^3/\text{s}$  from a 6-8 m diameter vent (D. J. Geist  
250 et al., 2008a). D. J. Geist et al. (2008a) employ the Head and Wilson (1987) single va-  
251 por phase model to estimate the volatile content and vent diameter on day 7 to be 0.1  
252 to 0.2 weight % water.

253 We extend this approach to include both  $\text{H}_2\text{O}$  and  $\text{CO}_2$ . Specifically, our model  
254 assumes a cylindrical conduit, laminar flow up to the magma fragmentation threshold,  
255 fixed inlet pressure, and equilibrium  $\text{H}_2\text{O}$  and  $\text{CO}_2$  degassing for a Sierra Negra com-  
256 position derived from MELTS (Gualda et al., 2012; Ghiorso & Gualda, 2015). (Model  
257 details and code verification tests are given in the Supplemental Material.)

258 Parfitt et al. (1995) note that lava ponding, drain back, and bubble coalescence can  
259 all decrease the observed height relative to predictions from the Head and Wilson (1987)  
260 model. Figure 6A,B in Parfitt et al. (1995) shows that for a volume flux of  $100 \text{ m}^3/\text{s}$ ,  
261 an eruption height of 50 m would be decreased by no more than 50% by these effects.  
262 So, we consider volatile compositions that would result in a fountain height of 100 m to  
263 account for these potential effects and obtain a maximum volatile composition.

264 Predicted fountain heights depend on both  $\text{H}_2\text{O}$  and  $\text{CO}_2$  content, but because wa-  
265 ter is so much more soluble, the compressibility of magma in the chamber depends pri-  
266 marily on  $\text{CO}_2$  content (Figure 5B). Thus, an upper bound on  $\beta_m$  is achieved with a lower  
267 value of water content (Figure 5A). A lower bound on water content from Koleszar et  
268 al. (2009) and Peterson et al. (2017) is 0.4 wt. %. From Figure 5A, a fountain height of  
269 100 m is obtained with  $\sim 600 \text{ ppm CO}_2$ , which corresponds to a compressibility of  $\sim 1.3 \times$   
270  $10^{-10} \text{ Pa}^{-1}$ . This is consistent with the estimate based on olivine melt inclusions.

271 Given that the MELTS-derived compressibility for bubble-free basalt is  $5.6 \times 10^{-11} \text{ Pa}^{-1}$ ,  
272 we suggest that a plausible lower bound on magma chamber volume is roughly a factor  
273 of two less than the upper bound. It should be noted, however, that the magma cham-  
274 ber may have been stratified with more gas rich magma toward the top. This could help  
275 explain the higher fire fountains observed at the onset of the 2005 eruption.

276 Thermal considerations presumably also place a lower bound on the magma cham-  
 277 ber volume: A very thin sill would likely freeze between recharge events. However, ap-  
 278 parently continuous recharge complicates such an analysis, which we defer to future stud-  
 279 ies.

### 280 4.3 An Estimate From Erupted Volume

281 From the product  $V\beta_m$ , we can obtain an estimation of the magma-chamber com-  
 282 pressibility ratio  $\eta \equiv \beta_m/\beta_c = V\beta_m/\Psi$ . With a fault dip of  $88^\circ\text{N}$  we find  $\eta \simeq 0.25$ .  
 283 Alternatively,  $\eta$  can be estimated from the ratio of the erupted volume to the geodetically-  
 284 inferred chamber volume change during the eruption:  $\eta = \Delta V_{erupt}/\Delta V - 1$  (Segall,  
 285 2010). S.-H. Yun (2007) estimates the volume change for the 2005 eruption  $\Delta V$  to be  
 286  $0.124 \text{ km}^3$  and the volume of lava that flowed into the caldera  $\Delta V_{erupt}$  to be  $0.141 \text{ km}^3$ .  
 287 D. J. Geist et al. (2008b), includes lava outside the caldera and estimates  $\Delta V_{erupt} = 0.15$   
 288  $\text{km}^3$ . Taking the larger value we find  $\eta \simeq 0.21$ , 16% smaller than the estimate based  
 289 on trapdoor faulting. This change in  $\eta$  reduces the upper bound on chamber volume from  
 290  $17.4$  to  $14.6 \text{ km}^3$ , for the best-fitting fault dip. Note that this approach provides an in-  
 291 dependent estimate of the chamber volume as it does not require trapdoor faulting, but  
 292 simply the erupted and geodetic volume change, as well as magma compressibility.

293 Finally, it should be noted that while  $\eta$  is a dimensionless parameter,  $\Psi$  is inversely  
 294 proportional to the shear modulus  $\mu$ . As a result, the estimation of  $V$  ( $V = \eta\Psi/\beta_m$ )  
 295 is also inversely proportional to  $\mu$ .

### 296 4.4 Relation to Other Volume Estimates

297 Body wave tomographic models beneath the Sierra Negra caldera have poor res-  
 298 olution in the shallow crust (less than 3 km depth) and therefore cannot resolve the magma  
 299 chamber (Tepp et al., 2014). The 3D attenuation model identifies a shallow magma body  
 300 between 0.5 km to 3 km below sea-level (Rodd et al., 2016), which is not inconsistent  
 301 with our estimate of 623 meter sill thickness.

## 5 Conclusions

We have placed bounds on the total volume of the Sierra Negra volcano in the Galapagos by modeling the fault-chamber interaction during the trap-door faulting event on April 16, 2005. Our main findings are:

1. The best-fitting faults are near vertical and dip steeply to the north,  $88^\circ$ .
2. An upper bound on chamber volume is between  $13.6 \text{ km}^3$  and  $20.6 \text{ km}^3$ , depending on fault dip. For the best fitting dip the volume is  $17.4 \text{ km}^3$ . (These estimates are for a shear modulus of 10 MPa;  $V$  is inversely proportional  $\mu$ .)
3. The lower bound on volume is roughly one-half the upper bound.
4. These estimates are consistent with those obtained from the ratio of the erupted volume to geodetically determined change in magma chamber volume.

## Acknowledgments

The research was supported by grants from the National Science Foundation Division of Earth Science (EAR-1829763). The InSAR and GPS data used can be downloaded from <https://doi.org/10.5281/zenodo.5225160>. The authors would like to thank helpful discussions with Dennis Geist, Mike Stock, and others.

## References

- Amelung, F., Jonsson, S., Zebker, H., & Segall, P. (2000, 10 26). Widespread uplift and /‘trapdoor/’ faulting on galapagos volcanoes observed with radar interferometry. *Nature*, *407*(6807), 993–996. Retrieved from <http://dx.doi.org/10.1038/35039604>
- Anderson, K. R., Johanson, I. A., Patrick, M. R., Gu, M., Segall, P., Poland, M. P., ... Miklius, A. (2019). Magma reservoir failure and the onset of caldera collapse at kilauea volcano in 2018. *Science*, *366*(6470).
- Anderson, K. R., Poland, M. P., Johnson, J. H., & Miklius, A. (2015). Episodic deflation-inflation events at kilauea volcano and implications for the shallow magma system. *Hawaiian Volcanoes: From Source to Surface*, 208, 229.
- Bell, A. F., La Femina, P. C., Ruiz, M., Amelung, F., Bagnardi, M., Bean, C. J., ... others (2021). Caldera resurgence during the 2018 eruption of sierra negra volcano, galápagos islands. *Nature communications*, *12*(1), 1–9.

- 332 Chadwick, W. W., Geist, D. J., Jónsson, S., Poland, M., Johnson, D. J., &  
 333 Meertens, C. M. (2006). A volcano bursting at the seams: inflation, faulting,  
 334 and eruption at sierra negra volcano, galápagos. *Geology*, *34*(12), 1025–1028.
- 335 Denlinger, R. P. (1997). A dynamic balance between magma supply and eruption  
 336 rate at kilauea volcano, hawaii. *Journal of Geophysical Research: Solid Earth*,  
 337 *102*(B8), 18091–18100.
- 338 Geist, D., White, W. M., Albarede, F., Harpp, K., Reynolds, R., Blichert-Toft, J., &  
 339 Kurz, M. D. (2002). Volcanic evolution in the galápagos: The dissected shield  
 340 of volcan ecuador. *Geochemistry, Geophysics, Geosystems*, *3*(10), 1–of.
- 341 Geist, D. J., Harpp, K. S., Naumann, T. R., Poland, M., Chadwick, W. W.,  
 342 Hall, M., & Rader, E. (2008a). The 2005 eruption of Sierra Negra vol-  
 343 cano, Galápagos, Ecuador. *Bulletin of Volcanology*, *70*(6), 655–673. doi:  
 344 10.1007/s00445-007-0160-3
- 345 Geist, D. J., Harpp, K. S., Naumann, T. R., Poland, M., Chadwick, W. W., Hall,  
 346 M., & Rader, E. (2008b). The 2005 eruption of sierra negra volcano,  
 347 galápagos, ecuador. *Bulletin of Volcanology*, *70*(6), 655–673.
- 348 Gerlach, T. M., & Graeber, E. J. (1985). Volatile budget of Kilauea volcano. *Nature*,  
 349 *313*(6000), 273–277. doi: 10.1038/313273a0
- 350 Ghiorso, M. S., & Gualda, G. A. (2015). An H<sub>2</sub>O–CO<sub>2</sub> mixed fluid saturation model  
 351 compatible with rhyolite-MELTS. *Contributions to Mineralogy and Petrology*,  
 352 *169*(6), 1–30. doi: 10.1007/s00410-015-1141-8
- 353 Gualda, G. A., Ghiorso, M. S., Lemons, R. V., & Carley, T. L. (2012). Rhyolite-  
 354 MELTS: A modified calibration of MELTS optimized for silica-rich, fluid-  
 355 bearing magmatic systems. *Journal of Petrology*, *53*(5), 875–890. doi:  
 356 10.1093/petrology/egr080
- 357 Head, J. W., & Wilson, L. (1987). Lava fountain heights at pu’u ’0’o, Kilauea,  
 358 Hawaii. *Journal of Geophysical Research*, *92*(B13), 13715–13719. doi:doi:10  
 359 .1029/JB092iB13p13715
- 360 Johnson, D. J. (1992). Dynamics of magma storage in the summit reservoir of ki-  
 361 lauea volcano, hawaii. *Journal of Geophysical Research: Solid Earth*, *97*(B2),  
 362 1807–1820.
- 363 Jónsson, S. (2009, 6 9). Stress interaction between magma accumulation and trap-  
 364 door faulting on sierra negra volcano, galápagos. *Tectonophysics*, *471*(1–2),

- 365 36–44. Retrieved from [http://www.sciencedirect.com/science/article/  
366 pii/S0040195108003880](http://www.sciencedirect.com/science/article/pii/S0040195108003880) doi: <http://dx.doi.org/10.1016/j.tecto.2008.08.005>
- 367 Jónsson, S., Zebker, H., & Amelung, F. (2005, 6 15). On trapdoor faulting at  
368 sierra negra volcano, galápagos. *Journal of Volcanology and Geothermal Re-  
369 search*, 144(1–4), 59–71. Retrieved from [http://www.sciencedirect.com/  
370 science/article/pii/S0377027304004160](http://www.sciencedirect.com/science/article/pii/S0377027304004160) doi: [http://dx.doi.org/10.1016/  
371 j.jvolgeores.2004.11.029](http://dx.doi.org/10.1016/j.jvolgeores.2004.11.029)
- 372 Koleszar, A. M., Saal, A. E., Hauri, E. H., Nagle, A. N., Liang, Y., & Kurz, M. D.  
373 (2009). The volatile contents of the Galapagos plume; evidence for H<sub>2</sub>O and F  
374 open system behavior in melt inclusions. *Earth and Planetary Science Letters*,  
375 287(3–4), 442–452. doi: 10.1016/j.epsl.2009.08.029
- 376 Lees, J. M. (2007). Seismic tomography of magmatic systems. *Journal of Vol-  
377 canology and Geothermal Research*, 167(1), 37–56. Retrieved from [https://  
378 www.sciencedirect.com/science/article/pii/S0377027307001965](https://www.sciencedirect.com/science/article/pii/S0377027307001965) (Large  
379 Silicic Magma Systems) doi: <https://doi.org/10.1016/j.jvolgeores.2007.06.008>
- 380 Maerten, F., Resor, P., Pollard, D., & Maerten, L. (2005). Inverting for slip on  
381 three-dimensional fault surfaces using angular dislocations. *Bulletin of the  
382 Seismological Society of America*, 95(5), 1654–1665.
- 383 Mogi, K. (1958). Relations between the eruptions of various volcanoes and the defor-  
384 mations of the ground surfaces around them. *Earthq Res Inst*, 36, 99–134.
- 385 Murase, T., & McBirney, A. R. (1973). Properties of some common igneous rocks  
386 and their melts at high temperatures. *Geological Society of America Bulletin*,  
387 84(11), 3563–3592.
- 388 Okada, Y. (1992). Internal deformation due to shear and tensile faults in a half-  
389 space. *Bulletin of the seismological society of America*, 82(2), 1018–1040.
- 390 Parfitt, E. A., Wilson, L., & Neal, C. A. (1995). Factors influencing the height of  
391 Hawaiian lava fountains: implications for the use of fountain height as an in-  
392 dicator of magma gas content. *Bulletin of Volcanology*, 57(6), 440–450. doi:  
393 10.1007/BF00300988
- 394 Paulatto, M., Annen, C., Henstock, T. J., Kiddle, E., Minshull, T. A., Sparks, R.,  
395 & Voight, B. (2012). Magma chamber properties from integrated seismic  
396 tomography and thermal modeling at montserrat. *Geochemistry, Geophysics,  
397 Geosystems*, 13(1).

- 398 Peterson, M. E., Saal, A. E., Kurz, M. D., Hauri, E. H., Blusztajn, J. S., Harpp,  
399 K. S., ... Geist, D. J. (2017). Submarine basaltic glasses from the Galapagos  
400 Archipelago: Determining the volatile budget of the mantle plume. *Journal of*  
401 *Petrology*, 58(7), 1419–1450. doi: 10.1093/petrology/egx059
- 402 Pietruszka, A. J., & Garcia, M. O. (1999). The size and shape of kilauea volcano's  
403 summit magma storage reservoir: a geochemical probe. *Earth and Planetary*  
404 *Science Letters*, 167(3-4), 311–320.
- 405 Rawlinson, N., Fichtner, A., Sambridge, M., & Young, M. K. (2014). Seismic tomog-  
406 raphy and the assessment of uncertainty. *Advances in geophysics*, 55, 1–76.
- 407 Reynolds, R. W., Geist, D., & Kurz, M. D. (1995, 12). Physical volcanology and  
408 structural development of sierra negra volcano, isabela island, galápagos  
409 archipelago. *Geological Society of America Bulletin*, 107(12), 1398–1410.  
410 Retrieved from [http://gsabulletin.gsapubs.org/content/107/12/](http://gsabulletin.gsapubs.org/content/107/12/1398.abstract)  
411 [1398.abstract](http://gsabulletin.gsapubs.org/content/107/12/1398.abstract)
- 412 Rodd, R. L., Lees, J. M., & Tepp, G. (2016). Three-dimensional attenuation model  
413 of sierra negra volcano, galápagos archipelago. *Geophysical Research Letters*,  
414 43(12), 6259–6266.
- 415 Segall, P. (2010). *Earthquake and volcano deformation*. Princeton University Press.
- 416 Segall, P. (2013). Volcano deformation and eruption forecasting. *Geological Society,*  
417 *London, Special Publications*, 380(1), 85–106.
- 418 Segall, P., & Anderson, K. (2021). Repeating caldera collapse events constrain  
419 fault friction at the kilometer scale. *Proceedings of the National Academy of*  
420 *Sciences*, 118(30).
- 421 Segall, P., Cervelli, P., Owen, S., Lisowski, M., & Miklius, A. (2001). Constraints  
422 on dike propagation from continuous gps measurements. *Journal of Geophysi-*  
423 *cal Research: Solid Earth*, 106(B9), 19301–19317.
- 424 Tepp, G., Ebinger, C. J., Ruiz, M., & Belachew, M. (2014). Imaging rapidly de-  
425 forming ocean island volcanoes in the western galápagos archipelago, ecuador.  
426 *Journal of Geophysical Research: Solid Earth*, 119(1), 442–463.
- 427 Vasconez, F. J., Ramón, P., Hernandez, S., Hidalgo, S., Bernard, B., Ruiz, M., ...  
428 Ruiz, G. (2018). The different characteristics of the recent eruptions of fer-  
429 nandina and sierra negra volcanoes (galápagos, ecuador). *Volcanica*, 1(2),  
430 127–133.

- 431 Wasser, V. K., Lopez, T. M., Anderson, K. R., Izbekov, P. E., & Freymueller, J. T.  
432 (2021). Multidisciplinary Constraints on Magma Compressibility, the Pre-  
433 Eruptive Exsolved Volatile Fraction, and the H<sub>2</sub>O/CO<sub>2</sub> Molar Ratio for the  
434 2006 Augustine Eruption, Alaska. *Geochemistry, Geophysics, Geosystems*,  
435 *22*(9), 1–24. doi: 10.1029/2021gc009911
- 436 Yamakawa, N. (1955). On the strain produced in a semi-infinite elastic solid by an  
437 interior source of stress. *J. Seismol. Soc. Japan, Ser. 2*, *8*(2), 84–98. Retrieved  
438 from <https://ci.nii.ac.jp/naid/20001343438/en/>
- 439 Yun, S., Segall, P., & Zebker, H. (2006, 2 1). Constraints on magma chamber  
440 geometry at sierra negra volcano, galápagos islands, based on insar observa-  
441 tions. *Journal of Volcanology and Geothermal Research*, *150*(1–3), 232–243.  
442 Retrieved from [http://www.sciencedirect.com/science/article/pii/](http://www.sciencedirect.com/science/article/pii/S0377027305002611)  
443 [S0377027305002611](http://www.sciencedirect.com/science/article/pii/S0377027305002611) doi: <http://dx.doi.org/10.1016/j.jvolgeores.2005.07.009>
- 444 Yun, S.-H. (2007). *A mechanical model of the large-deformation 2005 sierra negra*  
445 *volcanic eruption derived from insar measurements*. Stanford University.